

Article

Combination Mechanism of Soil Dissolved Organic Matter and Cu^{2+} in Vegetable Fields, Forests and Dry Farmland in Lujiang County

Youru Yao ¹, Jingyi Zhang ¹, Kang Ma ¹, Jing Li ^{2,*}, Xin Hu ³, Yusi Wang ¹, Yuesheng Lin ¹, Fengman Fang ¹ and Shiyin Li ^{4,5,*}

¹ Key Laboratory of Earth Surface Processes and Regional Response in the Yangtze-Huaihe River Basin, Anhui Province, School of Geography and Tourism, Anhui Normal University, Wuhu 241002, China; yaoyouru@ahnu.edu.cn (Y.Y.); zjy@ahnu.edu.cn (J.Z.); 1921011181@ahnu.edu.cn (K.M.); wangyusi@ahnu.edu.cn (Y.W.); lys1213@ahnu.edu.cn (Y.L.); ffm1974@mail.ahnu.edu.cn (F.F.)

² Key Laboratory of Agro-Environment in Downstream of Yangtze Plain, National Agricultural Experiment Station for Agricultural Environment, Institute of Agricultural Resources and Environment, Jiangsu Academy of Agricultural Sciences, Nanjing 210014, China

³ Center for Microscopy and Analysis, Nanjing University of Aeronautics and Astronautics, Nanjing 210016, China; huxinma@nuaa.edu.cn

⁴ School of Environment, Nanjing Normal University, Nanjing 210023, China

⁵ Jiangsu Center for Collaborative Innovation in Geographical Information Resource Development and Application, Nanjing 210023, China

* Correspondence: lijing@jaas.ac.cn (J.L.); lishiyin@njnu.edu.cn (S.L.)

Abstract: Dissolved organic matter (DOM) serves as a critical link in the migration and transformation of heavy metals at the soil–solid interface, influencing the migration behaviour and transformation processes of Cu^{2+} in soil. There have been studies on the combination mechanisms between DOM and Cu^{2+} in paddy soils. However, the adsorption/complexation and redox processes between DOM and Cu^{2+} in other agricultural soil types (such as dry farmland and vegetable fields) are unclear. In order to reveal the combination process of DOM with Cu in different agricultural soil types and the dynamic changes in chemical behaviour that occur, this study analysed the variability of DOM components and structure in three soils using three-dimensional fluorescence spectroscopy and X-ray photoelectron spectroscopy. In addition, the priority order of different DOM compounds in combination with Cu and the change process in relation to the Cu valence state in the soil of Lujiang County, Anhui Province, was revealed based on laboratory experiments. The results showed that the composition of soil DOM was mainly composed of humic-like and fulvic-like substances with a clear terrestrial origin and that the organic matter showed a high degree of decomposition characteristics. The results indicated that the composition of soil DOM is mainly composed of humic and fulvic acid-like substances, and they have obvious characteristics of terrestrial origin. In addition, the soil organic matter showed high decomposition characteristics. The complex stability constants ($\lg K_M$) of humic acid-like substances with Cu^{2+} follow the order of forest land ($\lg K_M = 5.21$), vegetable land ($\lg K_M = 4.90$), and dry farmland ($\lg K_M = 4.88$). The $\lg K_M$ of fulvic acid-like substances with Cu^{2+} is in the order of dry farmland ($\lg K_M = 4.51$) and vegetable land ($\lg K_M = 4.39$). Humic acid-like substances in soil DOM combine preferentially with Cu^{2+} , showing a stronger chelating affinity than fulvic acid-like substances. Cu^{2+} complexes mainly include hydroxyl, phenolic hydroxyl and amino functional groups are included in soil DOM, accompanied by redox reactions. In comparison to dry farmland, the soil DOM in forest and vegetable fields undergoes more intense redox reactions simultaneously with the chelation of Cu^{2+} . Therefore, the application of organic fertilisers to vegetable and forest soils may lead to uncertainties concerning the fate of heavy metals with variable chemical valence. These results contribute to a deeper understanding of the interaction mechanisms between DOM and Cu^{2+} in agricultural soils.

Keywords: dissolved organic matter; copper; combination mechanism; humic acid-like substances



Citation: Yao, Y.; Zhang, J.; Ma, K.; Li, J.; Hu, X.; Wang, Y.; Lin, Y.; Fang, F.; Li, S. Combination Mechanism of Soil Dissolved Organic Matter and Cu^{2+} in Vegetable Fields, Forests and Dry Farmland in Lujiang County. *Agriculture* **2024**, *14*, 684. <https://doi.org/10.3390/agriculture14050684>

Academic Editor: Daniel G. Strawn

Received: 20 March 2024

Revised: 25 April 2024

Accepted: 26 April 2024

Published: 27 April 2024



Copyright: © 2024 by the authors. Licensee MDPI, Basel, Switzerland. This article is an open access article distributed under the terms and conditions of the Creative Commons Attribution (CC BY) license (<https://creativecommons.org/licenses/by/4.0/>).

1. Introduction

With the rapid development of the mining industry, concerns about copper (Cu) contamination in the soil near mining areas have attracted increasing global attention [1]. The levels of Cu contamination in the vicinity of mining areas in Oman, China, Australia, and the United Kingdom are of concern [2]. In addition, Cu poses a significant ecological risk to the soil surrounding mining areas, contributing 21.7% of the total risk [2]. In these areas, agricultural areas have higher Cu contamination than non-agricultural areas. As Cu levels in soil increase, its ecological toxicity can affect the growth and development of organisms, leading to reduced crop yields and even death, posing a risk to soil ecosystems [3]. It has been shown that anthropogenic activities (industrial, agricultural, and urbanisation) can not only elevate soil Cu concentrations and bioavailability but also lead to enrichment in the local biogenic skin (*Bufo spinosus*) in Algerian Riparian Areas [4]. Cu is an essential trace element for the growth and development of both animals and plants, serving as a major component of oxidase enzymes [5]. However, an excess of Cu in the soil can be transferred through the food chain to higher trophic levels, ultimately threatening ecological security and even causing direct harm to human health, including damage and mortality [6,7]. Therefore, the study of Cu migration and transformation in soil has become a focal point of current research in the field of environmental geochemistry.

Dissolved organic matter (DOM) refers to heterogeneous compounds that are capable of passing through a 0.45 µm pore size filter and contain numerous active functional groups (such as hydroxyl, phenolic hydroxyl, carboxyl, quinone, etc.) that can complex with heavy metals [8]. Soil structure, moisture, and organic matter can vary significantly between forest land, dry cropland, and vegetable land [9,10], resulting in DOM components with different expressions and structures of. Forest land typically has a good soil structure and moisture retention due to the stabilizing effect of tree root systems. Conventional tillage and irrigation in dryland areas may result in moisture loss. Vegetable land is subject to regular cultivation and management, which can reduce soil porosity and cause significant seasonal changes in moisture [10]. The molecular weight of DOM has been shown to decrease significantly with decreasing vegetation in dryland-to-grassland transition soil types [11]. In addition, the total relative abundance of lipids, proteins, and lignin increased significantly with the transition from meadow to grassland and desert steppe, while the relative abundance of carbohydrates, condensed aromatic hydrocarbons, and tannins decreasing significantly with the transition to grassland [11]. In contrast, the fraction of dissolved organic matter in forest soils is more closely related to temperature, microbial activity, and nutrient element content [12,13]. In the DOM of forest soils that experience long-term freezing and thawing, aromatic hydrocarbons were found to be the main compounds of DOM, accounting for 44.07%, followed by polycyclic aromatic hydrocarbons and polysaccharides [14]. In addition, under nutrient addition conditions, the content of hydrophilic fractions (tannins, polyphenols, oxidised polyphenols, and humus-bound carbohydrates) and hydrophobic fractions (aromatic compounds, paraffinic compounds, and amines) increased in the DOM of forest soils [15].

DOM influences the migration, transformation, and toxicity of heavy metals, especially Cu, in soils [16–18]. Studies indicate that electron-donating substituents (-OH, -NH₂) present in humic and fulvic acid-like components of the DOM in biomass char have strong ionic bonding with positively charged Cu²⁺ [19]. In addition, as the concentration of DOM in soil increases, the transformation of Cu shifts from unstable exchangeable forms to stable organic-bound and residual forms, with DOM inhibiting the migration of Cu in soil [20]. However, additional studies have confirmed that in soils with added manure, the increase in soil dissolved organic matter (DOM) promotes the mobility of Cu. This is because the addition of manure increases the content of aromatic carbon in the soil, and the formation of complexes between large aromatic carbon molecules and Cu enhances the mobility of Cu [21]. The types, structures, and properties of DOM generated during different composting periods (dominated by proteinaceous substances in the early stages and predominantly humic substances in the later stages) vary, thereby

affecting their chelating capacity with Cu [22]. There are significant differences in the binding of Cu with DOM from different sources and components, altering the mobility and availability of Cu. However, there is currently a lack of systematic research on the specific mechanisms underlying the interaction between agricultural soil DOM and Cu^{2+} , especially considering the varying degrees of anthropogenic influences on different agricultural soil cultivation practices. This leads to differences in the sources, composition, and structural characteristics of DOM, as well as variations in the combination processes and mechanisms between different components and Cu^{2+} . Further exploration and research are needed to fully understand this process. In addition, the differences in DOM components and the structures of different soil types are analyzed through practical cases to reveal the binding mechanism of DOM with Cu. The roles played by different DOM components in the binding process with Cu (accelerated migration/co-precipitation) can be clarified. Furthermore, by artificially regulating the component and structural changes to soil DOM, the transport behaviour of Cu can be inhibited and the bioavailability can be reduced to achieve the effect of controlling Cu pollution.

These differences in structure, moisture, and organic matter among agricultural soil may lead to variations in the structure and composition of DOM, thus obscuring its relationship with Cu. Lujiang County in Anhui Province, located in the transition zone between subtropical and temperate regions ($30^{\circ}57' \sim 31^{\circ}33' \text{ N}$, $117^{\circ}01' \sim 117^{\circ}34' \text{ E}$), is not only an important agricultural county in Anhui but also characterised by diverse agricultural land uses (dryland, vegetable growing, forests, etc.). In addition, the county is located in the Tan-Lu fault seismic zone, which is rich in non-ferrous metal deposits, and these mining activities pose a risk of soil contamination. Therefore, investigating the Cu content in different agricultural soils in Lujiang County and studying the combination processes and mechanisms between DOM from different sources and Cu^{2+} is essential to understanding Cu migration and transformation in different agricultural soils.

This study focused on dry farmland soil, vegetable field soil, and forest land soil in Lujiang County and investigated the morphological characteristics and source composition of DOM in soil. Various methods, including three-dimensional fluorescence spectroscopy, two-dimensional analysis, and X-ray photoelectron spectroscopy (XPS), were used to analyze the complexation processes and mechanisms between DOM and Cu^{2+} . The aim was to further elucidate the migration characteristics of Cu^{2+} in different agricultural soils and to provide new insights for the control of Cu pollution in agricultural soils.

2. Materials and Methods

2.1. Overview of the Study Area and Sample Collection

Lujiang County ($30^{\circ}57' \sim 31^{\circ}33' \text{ N}$, $117^{\circ}01' \sim 117^{\circ}34' \text{ E}$) is located in the central part of Anhui Province and has a relatively low elevation (Figure 1). The region is rich in agricultural land resources, covering a total agricultural land area of 123,429 hectares, accounting for approximately 52.66% of the county's total area. The county is also abundant in mineral resources, with a Cu reserve of 2.15 million tons, ranking second in Anhui Province. There are many iron ore mines, pyrite mines, aluminium mines, and polymetallic mines that have been established in Lujiang County (Figure 1). A total of 38 forest soil samples, 32 dry farmland samples, and 14 vegetable samples were collected (Figure 1). The forest soil type is Luvisols, and the overstorey vegetation is mainly dominated by trees of the *Coniferopsida* and *Camphoraceae* families. The soil type of the dry farmland and vegetable fields is Anthrosols, with wheat being the main crop in the dry farmland and *Chinese cabbage* and *radish* in the vegetable fields. Among them, the soil-forming parent material of forest soils, dry farmland soils, and vegetable fields was dominated by argillaceous rocks, and the soils of the three land use types were acidic ($\text{pH } 6.2 \pm 1.7$, 6.3 ± 0.9 , and 6.2 ± 1.4 , respectively), with soil organic matter contents of 11.65 ± 3.72 , 11.91 ± 4.33 , and $14.13 \pm 4.21 \text{ g/kg}$, respectively, and there was no statistical significance in the variability of the pH value ($p > 0.05$), and organic matter contents ($p > 0.05$) among the three types. The spatial distribution of Cu in the county is generally more in the south than in the north,

with an average content of $33.20 \pm 28.10 \text{ mg}\cdot\text{kg}^{-1}$, surpassing the background value of $21.6 \text{ mg}\cdot\text{kg}^{-1}$ in widespread areas.

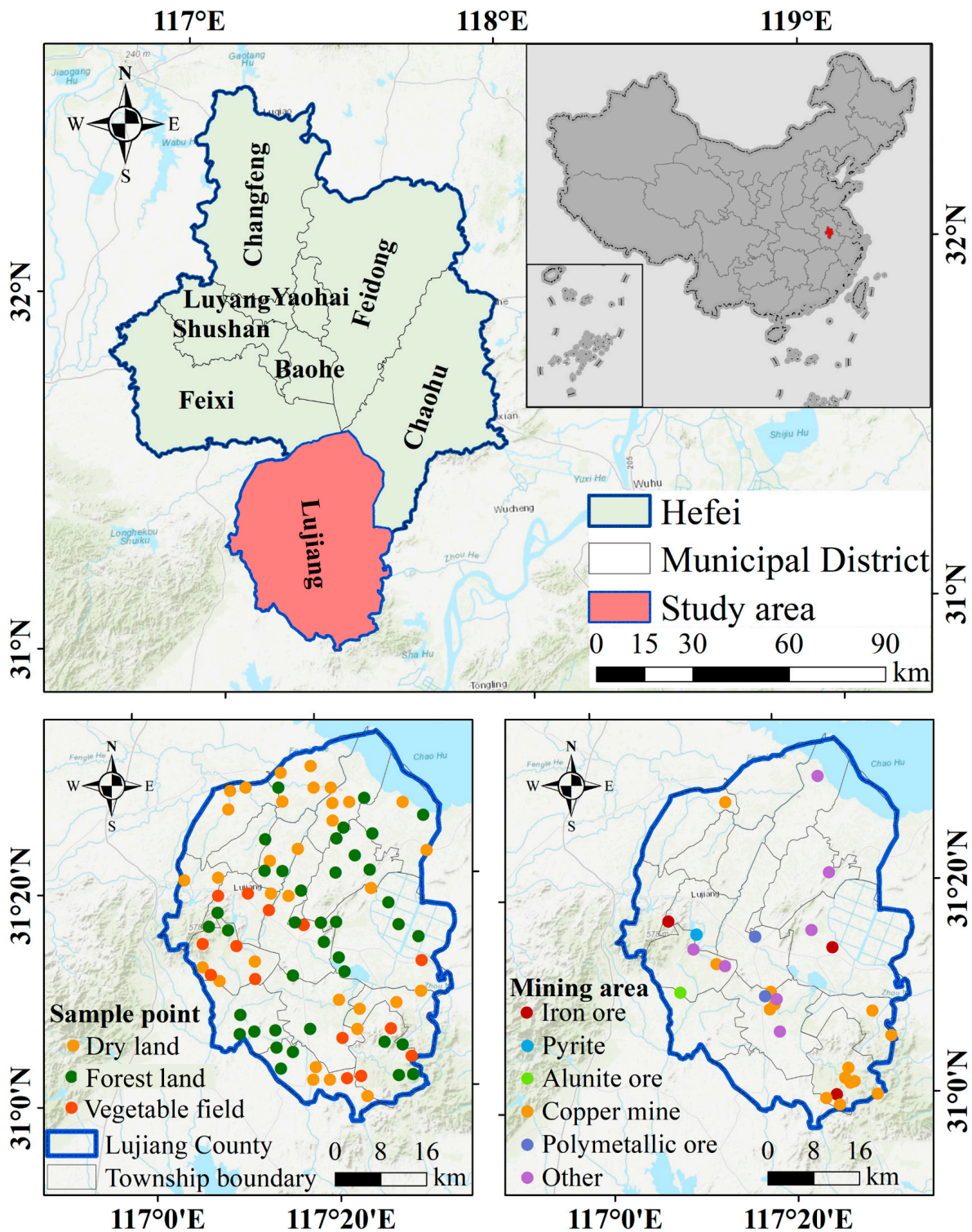


Figure 1. The figure shows the geographic location of the study area, distribution of mines, and distribution of sample points.

Sampling points were uniformly distributed in a $3 \text{ km} \times 3 \text{ km}$ grid, and a cloverleaf-type sampling method was used to collect surface soil samples (0–20 cm) at each point. A total of 14 soil samples were collected from vegetable fields, 35 from dry farmland, and

35 from surface forest land. The collected samples were air-dried for 30 d, broken into pieces, and sieved through 2 mm and 0.149 mm screens (nylon sieve).

2.2. Extraction and Analysis of DOM

The sieved soil samples were mixed with ultrapure water at a solid-to-liquid ratio of 1:10 (*w:v*) [23,24]. The mixture was shaken at $220 \text{ r}\cdot\text{min}^{-1}$ for 24 h at $25 \text{ }^{\circ}\text{C}$ with agitation. After the completion of shaking, the samples were centrifuged at 4000 rpm for 30 min, and the supernatant was collected. The supernatant was filtered through a $0.45 \text{ }\mu\text{m}$ glass fibre filter membrane to obtain the DOM solution. The filtrate was then transferred to a 500 mL amber glass bottle and stored in the dark at $4 \text{ }^{\circ}\text{C}$ in a refrigerator. Samples for machine measurement were analyzed within 24 h. A portion of the original DOM solution was centrifuged and dried using a vacuum freeze dryer (FD-1A-50, BaYue, Changsha, China) for subsequent analysis.

2.3. Complexometric Titration of DOM and Cu^{2+}

To avoid filtration effects, the DOM solution was diluted to a concentration of $10.0 \text{ mg}\cdot\text{L}^{-1}$. The pH of the titration system was controlled using $0.1 \text{ mol}\cdot\text{L}^{-1}$ NaOH and HNO_3 solutions ($\text{pH} = 7.0 \pm 0.1$) to prevent precipitation. Concentrated CuSO_4 solution ($0.1 \text{ mol}\cdot\text{L}^{-1}$) was titrated into a 25 mL DOM solution, generating a series of titration samples. Different gradient concentrations of Cu^{2+} solution (0, 5, 10, 20, 30, 50, 75, and $100 \text{ }\mu\text{mol}\cdot\text{L}^{-1}$) were added to the titration samples [25]. The titration samples were kept in the dark at $25 \text{ }^{\circ}\text{C}$ for 24 h to achieve complexation equilibrium, and dynamic light scattering, three-dimensional fluorescence spectroscopy, and synchronous fluorescence analysis were conducted on the complexation solution.

2.4. Spectral Analysis

Fluorescence excitation–emission matrix (EEM) spectroscopy is a simple, sensitive, and non-destructive technique that can provide valuable information on the molecular structure of DOM. EEM spectroscopy in combination with bursting methods can be applied as a reliable technique for a better understanding of the binding properties of metal ions and fluorescent substances of DOM in soils [26]. Fluorescence spectra were measured using a fluorescence spectrophotometer (F97Pro, Shanghai Lingguang, Shanghai, China). The excitation wavelength (*Ex*) ranged from 200 to 450 nm (5 nm increment), and the emission wavelength (*Em*) ranged from 25 to 550 nm (5 nm increment). The scanning speed was $240 \text{ nm}\cdot\text{min}^{-1}$, and the slit width was set to 5 nm [27]. Synchronous fluorescence (FM-4P-TCSPC, HORIBA JY, Paris, France) was performed with an excitation wavelength range of 250 to 550 nm, a constant offset $\Delta\lambda$ of 60 nm, and both excitation and emission slit widths set at 5 nm. The scan speed was $240 \text{ nm}\cdot\text{min}^{-1}$. A 150 W ozone-free xenon arc lamp was used as the light source, and ultrapure water was used as the blank. The system automatically corrected for Rayleigh and Raman scattering.

UV-visible spectroscopy was used to analyze the complexation solution, with ultrapure water used as the blank. The absorption spectra were scanned in the wavelength range of 200 to 900 nm using a UV-visible spectrophotometer (Genesys 50, Thermo Scientific, Waltham, Massachusetts, USA), with a step size of 2 nm. The calculation formulas and parameter meanings for fluorescence index (FI), humification index (HIX), biological index (BIX), SUV_{254} , and EET/EBz are detailed in Table S1 of the Supplementary Materials (SI).

2.5. Characterisation Analysis

Scanning electron microscopy (SEM) (Gemini 300, Carl Zeiss AG, Oberkochen, Germany) with an accelerating voltage set between 0.02 and 30 kV was utilised to observe the surface morphology of dried DOM and the DOM- Cu^{2+} complex after the reaction [28]. Transmission electron microscopy (TEM) (JEOL 2100F, JEOL Corporation, Tokyo, Japan) with an accelerating voltage set at 200 kV was used to observe the morphology and particle size of DOM [28]. X-ray photoelectron spectroscopy (XPS) (ESCALab 250, Thermo Fisher

Scientific, Waltham, Massachusetts, USA) was used to characterise the surface elemental composition and chemical state of DOM.

2.6. Data Analysis

2.6.1. Two-Dimensional (2D-COS) Analysis

Based on the Noda theory [29] and the method provided by Ozaki [30], 2D Shige ver. 1.3 (Shigeaki Morita, Kwansai Gakuin University, Hyogo, Japan) was used for 2D-COS analysis of DOM-Cu²⁺, which generated two types of spectra: synchronous spectra and asynchronous spectra. These spectra were used to study their interaction mechanisms.

2.6.2. Complexation Parameter Fitting

The modified Stern–Volmer equation, as shown in Equation (1) [31], was used for complexation parameter fitting to estimate the complexation abilities of different fluorescence components in DOM with Cu²⁺.

$$\frac{F_0}{F_0 - F} = \frac{1}{f \times K_M \times C_M} + \frac{1}{f} \quad (1)$$

In Equation (1), F_0 and F represent the fluorescence intensity without and with the addition of different concentrations of Cu²⁺, respectively. f is the proportion of fluorescent groups capable of combining with Cu²⁺, K_M is the stability constant satisfying the complexation conditions, and C_M is the concentration of Cu²⁺.

2.6.3. Data Statistics

SPSS 20.0 software was utilised for data analysis and testing, while Origin 2019 and XPSPEAK41 software were used for graphical presentation. Non-parametric tests (one-sample K-S test) were used to test for differences between data sets.

3. Results and Discussion

3.1. DOM Spectral Characteristics and Source Analysis

3.1.1. UV-Visible Spectral Parameter Analysis

Analysis of UV-visible spectra of DOM in soil revealed that the SUV₂₅₄ value of DOM in forest soil was higher than that in other land use of soil. A higher SUV₂₅₄ value indicates a higher content of aromatic compounds in DOM [32]. Compared to the other two land use types, forest soil DOM in Lujiang County contains more aromatic compounds, and the aromaticity of soil humus is higher ($p = 0.001 < 0.05$) (Table 1). Studies indicate that aromatic substances produced by trees can undergo chemical reactions with soil and remain stable in the soil [33]. The SUV₂₆₀ value of forest soil DOM is greater than 4, while the SUV₂₆₀ values of vegetable field and dryland soil DOM are below 4. A higher SUV₂₆₀ value indicates a higher proportion of hydrophobic components in DOM, indicating stronger activity in the migration and transformation of pollutants [34]. This implies that the DOM components in forest soil are mainly composed of hydrophobic substances, while the DOM components in the other two types of agricultural soil are mainly composed of hydrophilic substances. This may be due to the higher content of aromatic substances in forest soil, which have strong hydrophobic properties [35]. Therefore, forest DOM exhibits hydrophobicity, which is consistent with the conclusion drawn from the SUVA₂₅₄ value. Although the variability in soil organic carbon content among the three land use types was not statistically significant, the structure of DOM in forest soils was different from the structure of DOM in the other two agricultural soils. This is because forest soils tend to have a richer vegetation cover, which can result in more organic matter being deposited on the soil surface. This organic matter may be more difficult for water to break down or dissolve under the influence of plant residues, making the soil more hydrophobic overall. In addition, forest soils tend to have higher levels of clay, and these components form a more stable structure in the soil, making it less permeable to water and more difficult for organic matter to be dissolved by water. In contrast, dry farmland and vegetable soils may be more susceptible to ploughing

or human disturbance, resulting in a looser soil structure and organic matter that is more soluble in water [10,11].

Table 1. The table shows UV-visible spectral parameters of soil dissolved organic matter for different land use systems.

Land Use System	SUVA ₂₅₄	SUVA ₂₆₀	E _{ET} /E _{Bz}	E ₄ /E ₆	E ₂ /E ₃
Dry farmland	2.32 ± 0.03 a	2.21 ± 0.03 a	0.38 ± 0.01 a	3.21 ± 0.87 a	3.09 ± 0.08 a
Forest land	9.12 ± 0.03 b	8.75 ± 0.03 b	0.74 ± 0.01 b	4.04 ± 0.16 a	2.69 ± 0.04 a
Vegetable fields	2.22 ± 0.06 a	2.05 ± 0.06 a	0.15 ± 0.02 a	3.22 ± 0.21 a	3.90 ± 0.07 a

Note: Different letters represent differences at the 95% confidence level. Data in the table are mean values ± standard deviations.

The range of E_{ET}/E_{Bz} is related to the proportion of oxygen-containing functional groups in the aromatic structure of DOM [36]. The results show that the E_{ET}/E_{Bz} value of forest soil DOM is significantly higher than that of other types of agricultural soil DOM, indicating a higher proportion of oxygen-containing functional groups in its aromatic structure. The oxygen-containing functional groups on the surface of DOM directly affect its combination capacity with heavy metal ions [37]. Additionally, the E₄/E₆ value of forest soil DOM is greater than 4, indicating a higher degree of benzene ring carbon skeleton polymerisation and aromatisation. E₂/E₃ is used to characterise the relative molecular weight of DOM and is inversely proportional to the molecular weight of DOM [38]. The E₂/E₃ value of vegetable field soil (3.90 ± 0.07) is significantly higher than that of other types of agricultural soil, while the E₂/E₃ value of forest soil is the smallest (2.69 ± 0.04). This suggests that the molecular weight of forest soil DOM is larger, while the molecular weight of vegetable field DOM is smaller. Vegetable field soil, due to the large application of organic fertilisers such as livestock and poultry manure, has a relatively high natural source of DOM, and the molecular weight of DOM from such sources is generally smaller [39]. Moreover, with frequent plowing and good soil aeration, the decomposition of DOM is more thorough, leading to a smaller molecular weight [40]. In contrast, in forest soil, DOM mainly comes from the litter of woody plants, animal and plant residues, and microbial secretions. The lignin and cellulose of woody plants, under the action of microorganisms, not only decompose slowly but also are often not completely decomposed, resulting in a larger molecular weight in terms of DOM [41]. The DOM components of forest soils with high molecular weights and unsaturated oxidised or aromatic structures, such as aromatic and lignin substances, can preferentially bind to metals (Cu) through hydrophobic partitioning, hydrogen bonding, and electrostatic interactions [42].

3.1.2. The Fluorescence Components and Source of DOM in Different Agricultural Soils

Three-dimensional fluorescence spectroscopy was used to further analyze DOM in different types of agricultural soils. As shown in Figure 2, the three-dimensional fluorescence of dryland and vegetable field soil DOM is similar, with two fluorescence peaks, namely, humic-like fluorescence peak C1 (λ_{Ex}/λ_{Em} = 315/427 nm) and fulvic-like fluorescence peak C2 (λ_{Ex}/λ_{Em} = 245/500 nm); the humic-like fluorescence peak is C1 (λ_{Ex}/λ_{Em} = 315/434 nm) and the fulvic-like fluorescence peak is C2 (λ_{Ex}/λ_{Em} = 255/500 nm) [43,44]. The three-dimensional fluorescence spectrum of forest soil DOM shows only one fluorescence peak, which is the humic-like fluorescence peak of C1 (λ_{Ex}/λ_{Em} = 350/423 nm). Among the different land use types, forest soils are less affected by anthropogenic activities than dry farmland soils and vegetable soils, with the main components of DOM coming from the decomposition of plant litter itself. However, agricultural soils, dry farmland soils, and vegetable soils have been cultivated for a long time with inorganic and organic fertilisers, resulting in more DOM components than that of forest soils [39].

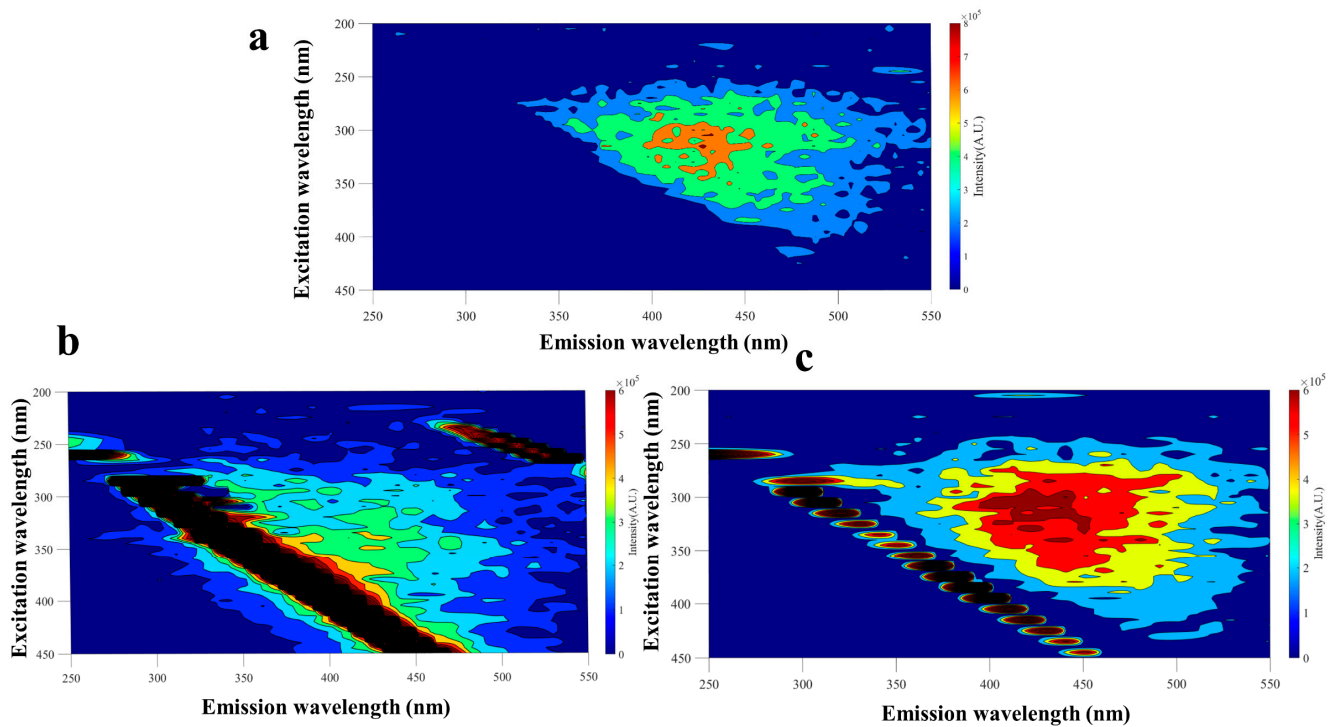


Figure 2. The figure shows the three-dimensional fluorescence spectral characteristics of dissolved organic matter in soils of different agricultural land use types: (a). dry farmland, (b). forest land, and (c). vegetable fields.

The values of FI, BIX, and HIX were employed to analyze the source characteristics and humification degree of soil DOM in different agricultural soils (Table S2). The FI values for dryland, forest land, and vegetable field overall approach 1.4, indicating that the external characteristics of soil DOM are very typical. BIX measures the proportion of autochthonous organic matter, with BIX values less than 1 indicating that the autochthonous source characteristic of DOM is not significant. The BIX values for different agricultural soils in Lujiang County are all less than 1. This suggests that the autochthonous source characteristic of soil DOM in agricultural soils is not significant. HIX reflects the degree of organic matter decomposition in the environment [45], where a higher HIX value indicates the higher of organic matter decomposition and aromaticity, as well as greater stability. The HIX values for soil DOM in different agricultural soils in Lujiang County are all greater than 6, with the order being forest land being higher than vegetable field and dryland. Therefore, compared with other types of agricultural soil DOM, the degree of organic matter decomposition and aromaticity of soil DOM in forest land are higher, consistent with the conclusions drawn from the changes in spectral parameters. The main reason for the differences in DOM structure between the different agricultural types is human activity, as vegetable and dryland soils are subject to long-term anthropogenic cultivation and the application of organic/inorganic fertilisers and regular ploughing disrupts the decomposition process of organic matter [46]. In contrast, forest soils are less cultivated, which favours the microbial decomposition of dead leaves, resulting in high decomposition and aromatisation of organic matter. In addition, forest soils typically have more complex and abundant microbial communities, which play an important role in the degradation and transformation of DOM. Microbial activity can facilitate the decomposition process of DOM, transforming it into more complex and aromatic organic matter. Soil microbial exoenzymes break down lignin in plant biomass into smaller, partially degraded lignin oligomers. These oligomers undergo oxidation to form unstable quinones, which can polymerise into high-molecular-weight humic substances [47].

3.2. Combination Process of Soil DOM with Cu^{2+} in Different Agricultural Soils

3.2.1. Fluorescence Quenching Characteristics of DOM at Different Cu^{2+} Concentrations

The fluorescence intensities of soil DOM in dryland, forest land, and vegetable field all decreased with increasing Cu^{2+} concentrations (Figure 3 and Figures S1–S3). When the added Cu^{2+} concentration was $100 \mu\text{mol}\cdot\text{L}^{-1}$, the F_{max} values of C1 (humic acid-like) and C2 (fulvic acid-like) in dryland soil DOM decreased by 59.3% and 55.9%, respectively. In vegetable field soil DOM, the F_{max} values of C1 and C2 decreased by 70% and 69.3%, respectively. These results indicate that both components present in dryland and vegetable field soil DOM can bind with Cu^{2+} , and there are differences in their combination modes. Among them, the combination strength of humic acid-like components is greater than that of fulvic acid-like components (Figure 3). As shown in Figure 3b, when the added Cu^{2+} concentration reached $100 \mu\text{mol}\cdot\text{L}^{-1}$ in forest land soil DOM solution, the F_{max} of C1 (humic acid-like) decreased by 54.6%, suggesting that the humic acid-like components in forest land soil DOM can combine with Cu^{2+} .

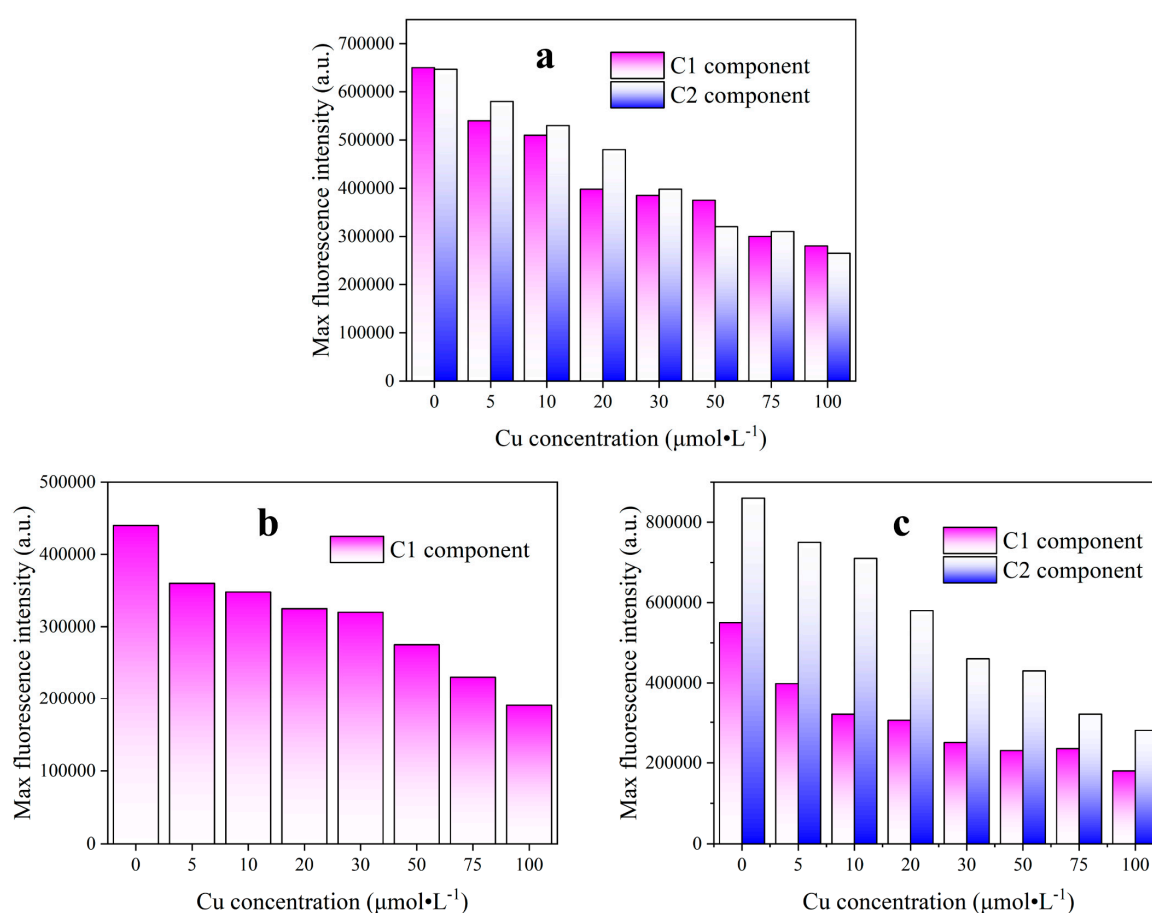


Figure 3. The figure shows the fluorescence quenching processes of different components in different agricultural soils under different Cu^{2+} concentrations (0, 5, 10, 20, 30, 50, 75, and $100 \mu\text{mol}\cdot\text{L}^{-1}$): (a). dry farmland, (b). forest land, and (c). vegetable fields. C1 is a humic acid-like component, and C2 is a fulvic acid-like component.

3.2.2. Kinetic fitting of DOM combines with Cu^{2+}

The combination stability constants ($\lg K_M$) of various fluorescent components in different agricultural soil DOM with Cu^{2+} , as well as the relationship between the combination fluorescence groups and Cu^{2+} concentration (C_M^{-1}), were fitted using the modified Stern–Volmer equation. The quenched fluorescence values of the three types of agricultural soil

DOM components showed a good linear relationship with C_M^{-1} ($1/Cu$ concentration) ($R^2 = 0.80-0.99$) (Figure 4 and Table 2).

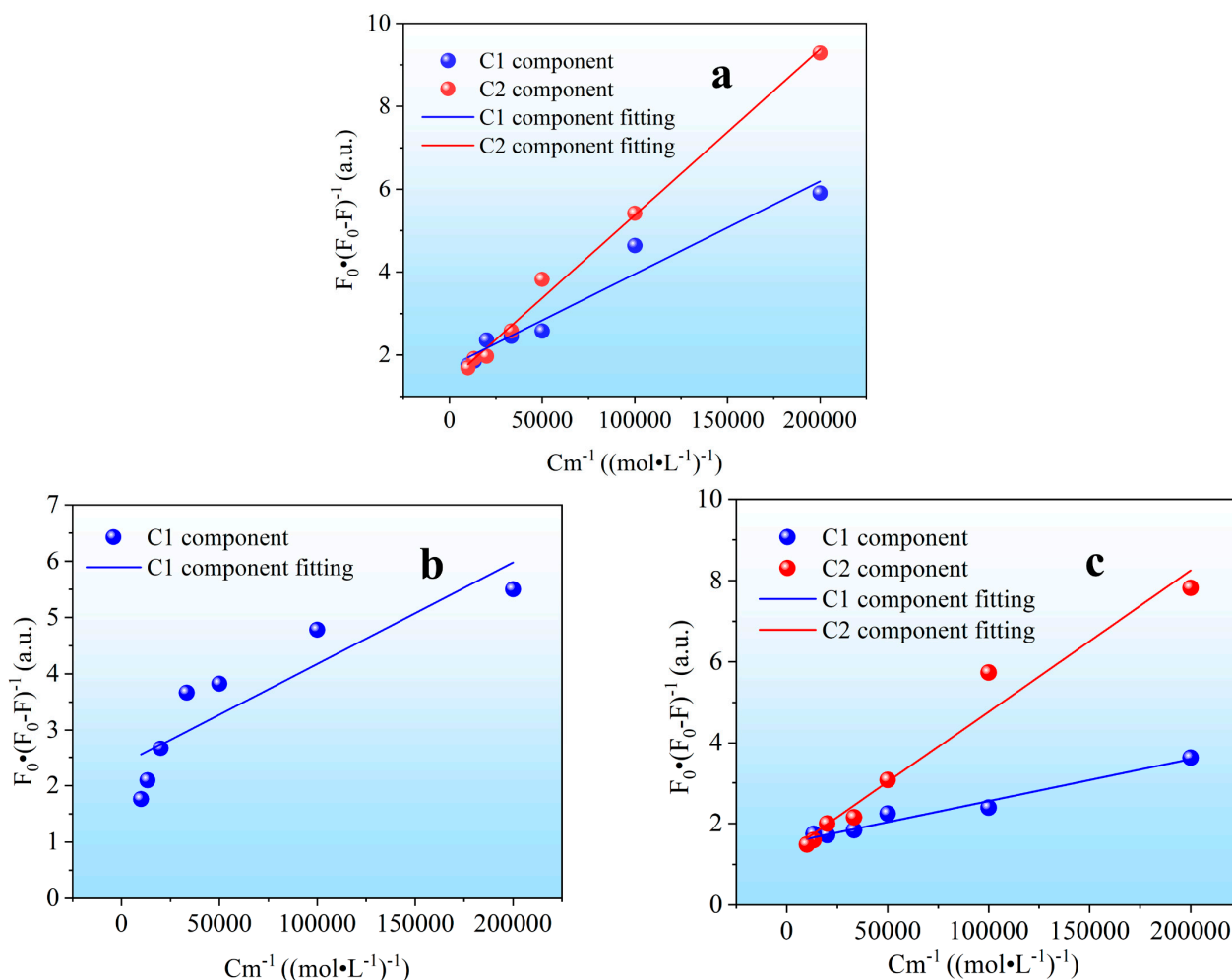


Figure 4. The figure shows the modified Stern–Volmer fitting of distribution bits of each component in three-dimensional fluorescence spectrum in different agricultural soils under different Cu^{2+} concentrations (0, 5, 10, 20, 30, 50, 75, and 100 $\mu mol \cdot L^{-1}$): (a). dry farmland, (b). forest land, and (c). vegetable fields.

Table 2. The table shows the modified Stern–Volmer parameter of distribution bits of each component in three-dimensional fluorescence spectrum in different agricultural soils under different Cu^{2+} concentrations (0, 5, 10, 20, 30, 50, 75, and 100 $\mu mol \cdot L^{-1}$). K_M is the combination stability constant and f is the proportion of quenchable fluorophores.

Type	Component	LgK_M	$f/\%$	R^2
Dry farmland	C1	4.88	0.64	0.91
	C2	4.51	0.58	0.95
Forest land	C1	5.21	0.76	0.80
Vegetable fields	C1	4.90	0.58	0.98
	C2	4.39	0.47	0.95

Note: C1 is a humic acid-like component, and C2 is a fulvic acid-like component.

The combination fitting curves of dryland and vegetable field DOM indicate that $C1 > C2$ (Figure 4a,c), suggesting that the humic acid-like component binds more strongly with Cu^{2+} than the fulvic acid-like component. Looking at the proportion of combination

fluorescence groups (f value), the humic acid-like component in DOM has a higher proportion of fluorescence groups coordinating with Cu^{2+} than the fulvic acid-like component. The combination fitting curve of forest land DOM (Figure 4b) suggests a strong combination affinity of the humic acid-like component in forest land DOM with Cu^{2+} .

The $\lg K_M$ values for the C1 component in agricultural soil DOM follow the order: forest land, vegetable field, and dryland (Table 2); however, for the C2 component, the order is dryland and vegetable field. This further illustrates the heterogeneity and asynchrony in the combination interactions between different components of agricultural soil DOM and Cu^{2+} . Previous studies indicate that with the accumulation of time, complex substituents will replace simple substituents in soil DOM, and these complex substituents often contain a large number of unsaturated bonds [48], which can serve as combination sites for Cu^{2+} . Since forest land soil is subjected to less anthropogenic disturbance, forest land DOM contains more complex substituents, and the higher proportion of hydrophobic components leads to higher $\lg K_M$ values compared to other types of agricultural soil DOM [34]. Except for forest land, the $\lg K_M$ values of C1 in other types of agricultural soil DOM are higher than C2, indicating a stronger combination affinity of the humic acid-like component with Cu^{2+} compared to the fulvic acid-like component. This may be related to the aromaticity and higher degree of organic matter decomposition of the humic acid-like component [49]. Simultaneously, the interaction between humic acid-like components and Cu^{2+} forms a multi-dentate complex, enhancing the combination between them [50]. The proportion of fluorescence groups coordinating with Cu^{2+} is highest in forest land DOM components because forest land soil DOM contains more oxygen-containing functional groups and has a higher aromaticity, thus enhancing the combination between soil DOM and Cu^{2+} through providing combination sites for cation- π interactions [51].

3.3. The Combination Mechanism of DOM with Cu^{2+}

3.3.1. Morphology and Structural Changes before and after Combining DOM with Cu^{2+}

To further investigate the changes in the surface morphology of different types of agricultural soil DOM after combination with Cu^{2+} , scanning analysis was conducted using SEM and TEM on dried combination powders (Figures 5 and 6).

Before combination with Cu, the particles of dryland soil DOM were aggregated, leading to tight connections between particles, uniform particle sizes, and a smooth surface (Figures 5a and 6a). After adding Cu^{2+} , the combination pores between the originally aggregated particles disappeared, becoming more compact. The particle diameter increased compared to the original DOM particles, transforming from small particle aggregates to a chunky structure. The molecular structure significantly enlarged, and the surface changed from smooth to rough (Figures 5b and 6b).

The surface structure of forest land soil DOM differed from dryland soil. Before combination with Cu, the surface structure of forest land soil DOM appeared layered, with noticeable internal fissures (Figures 5c and 6c). The DOM particles had a large molecular weight and a porous surface structure, and showed a clear aggregation with fractured edges. After adding Cu^{2+} , the external appearance of forest land soil DOM changed from loose to compact, the internal fissures disappeared, and the particles tightly bound together, transforming from fragmented to blocky structure (Figures 5d and 6d).

From the SEM and TEM images of vegetable field soil DOM, it can be observed that DOM had a smooth, small spherical structure with dense distribution, slightly rough surface, and apparent aggregation (Figures 5e and 6e). After adding Cu^{2+} , the surface morphology of vegetable field soil DOM changed from the original smooth spherical structure to irregular blocky structures bound together, with a significant increase in particle size (Figures 5f and 6f).

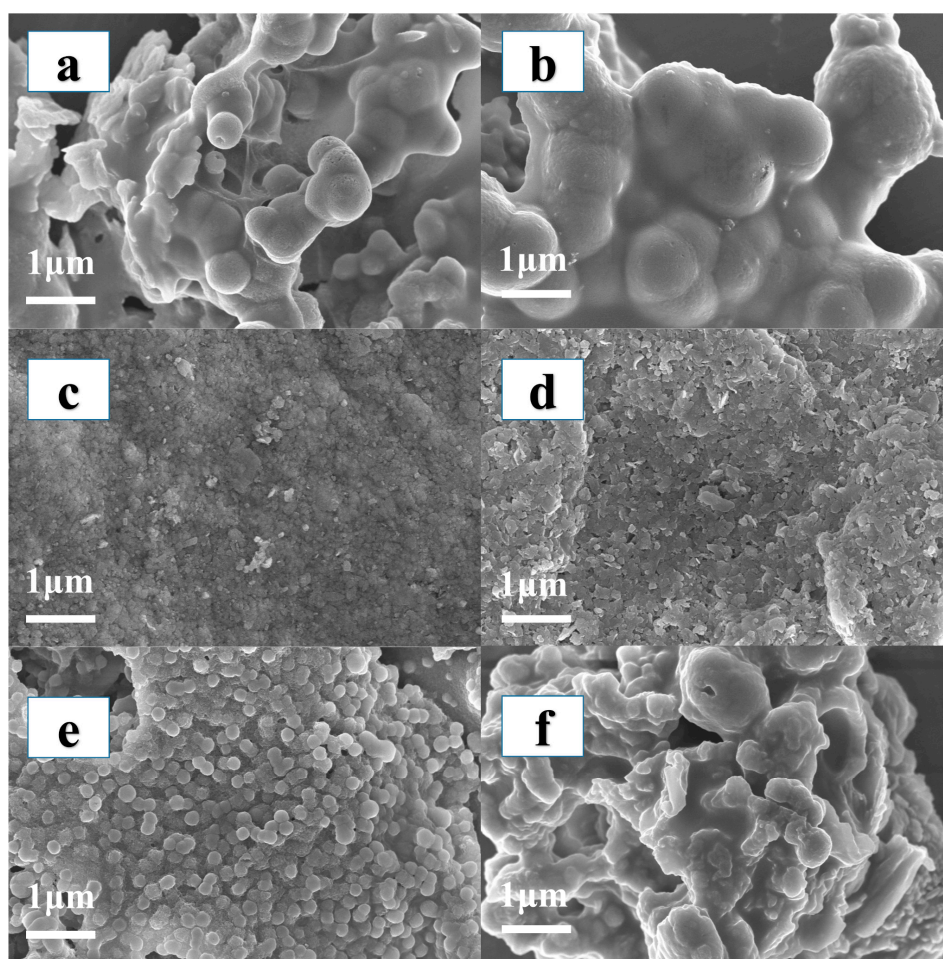


Figure 5. Scanning electron microscope (SEM) images of dissolved organic matter (DOM) being freeze-dried before and after combined with Cu^{2+} . (a). dryland samples before being combined with Cu, (b). dryland samples after combined with Cu, (c). forest soil samples before being combined with Cu, (d). forest soil samples after combined with Cu, (e). vegetable field soil samples before being combined with Cu, (f). vegetable field soil samples after combined with Cu. Cu concentration: $100 \text{ mg}\cdot\text{L}^{-1}$.

3.3.2. Effect of Surface Functional Groups on the Combination of DOM and Cu^{2+}

The synchronous fluorescence spectra of dryland soil DOM combination with Cu^{2+} are shown in Figure 7a. In the synchronous fluorescence spectra of DOM, the peaks appeared spontaneously at 345 nm, 370 nm, 400 nm, and 430 nm, all indicating orthogonal cross-peaks. Among them, 345 nm and 370 nm represent the humic acid components, and 400 nm and 430 nm represent the fulvic acid components. This suggests that the fluorescence intensity of these two components in dryland soil DOM is negatively correlated with the added Cu^{2+} concentration, indicating that each component of the DOM is highly sensitive to Cu^{2+} . The asynchronous fluorescence spectra of dryland soil DOM combined with Cu^{2+} are shown in Figure 7b. In the asynchronous spectrum, there are six negative cross-peaks and two positive cross-peaks in the upper left corner of the diagonal. The combination sequence of dryland DOM components with Cu^{2+} is $350 \text{ nm} \rightarrow 400 \text{ nm} \rightarrow 425 \text{ nm} \rightarrow 435 \text{ nm} \rightarrow 445 \text{ nm} \rightarrow 390 \text{ nm} \rightarrow 380 \text{ nm} \rightarrow 485 \text{ nm}$, indicating that short-wave fulvic acid \rightarrow long-wave fulvic acid \rightarrow long-wave humic acid, with short-wave fulvic acid components in soil DOM preferentially combine with Cu^{2+} . The synchronous fluorescence spectra of vegetable field soil DOM in combination with Cu^{2+} are shown in Figure 7c. The synchronous spectrum has spontaneous peaks mainly at 348 nm, 365 nm, 395 nm, 420 nm, and 480 nm. The first two peaks represent fulvic acid components, and the last

three peaks represent humic acid components. In the asynchronous spectrum (Figure 7d), there are eight negative cross-peaks and five positive cross-peaks in the upper left corner of the diagonal. The combination sequence of vegetable field DOM components with Cu^{2+} is 315 nm \rightarrow 405 nm \rightarrow 415 nm \rightarrow 440 nm \rightarrow 480 nm \rightarrow 360 nm \rightarrow 378 nm \rightarrow 345 nm \rightarrow 515 nm, indicating short-wave fulvic acid \rightarrow long-wave fulvic acid \rightarrow short-wave humic acid-long-wave humic acid, with short-wave fulvic acid components in soil DOM preferentially combining with Cu^{2+} . The synchronous spectra of forest land soil DOM in combination with Cu^{2+} are shown in Figure 7e, and there are six spontaneous peaks, where 360 nm represents fulvic acid components, and the remaining peaks represent humic acid components. All spontaneous peaks are orthogonal cross-peaks, indicating that the fluorescence intensity of forest land DOM components is also negatively correlated with the added Cu^{2+} concentration, showing strong sensitivity. In the asynchronous spectrum (Figure 7f), there are six negative cross-peaks and seven positive cross-peaks in the upper left corner of the diagonal. The combination sequence of forest land DOM components with Cu^{2+} is 350 nm \rightarrow 360 nm \rightarrow 395 nm \rightarrow 410 nm \rightarrow 425 nm \rightarrow 440 nm \rightarrow 465 nm \rightarrow 475 nm \rightarrow 450 nm \rightarrow 415 nm \rightarrow 360 nm \rightarrow 305 nm \rightarrow 490 nm, indicating short-wave fulvic acid \rightarrow long-wave fulvic acid \rightarrow short-wave humic acid-long-wave humic acid.

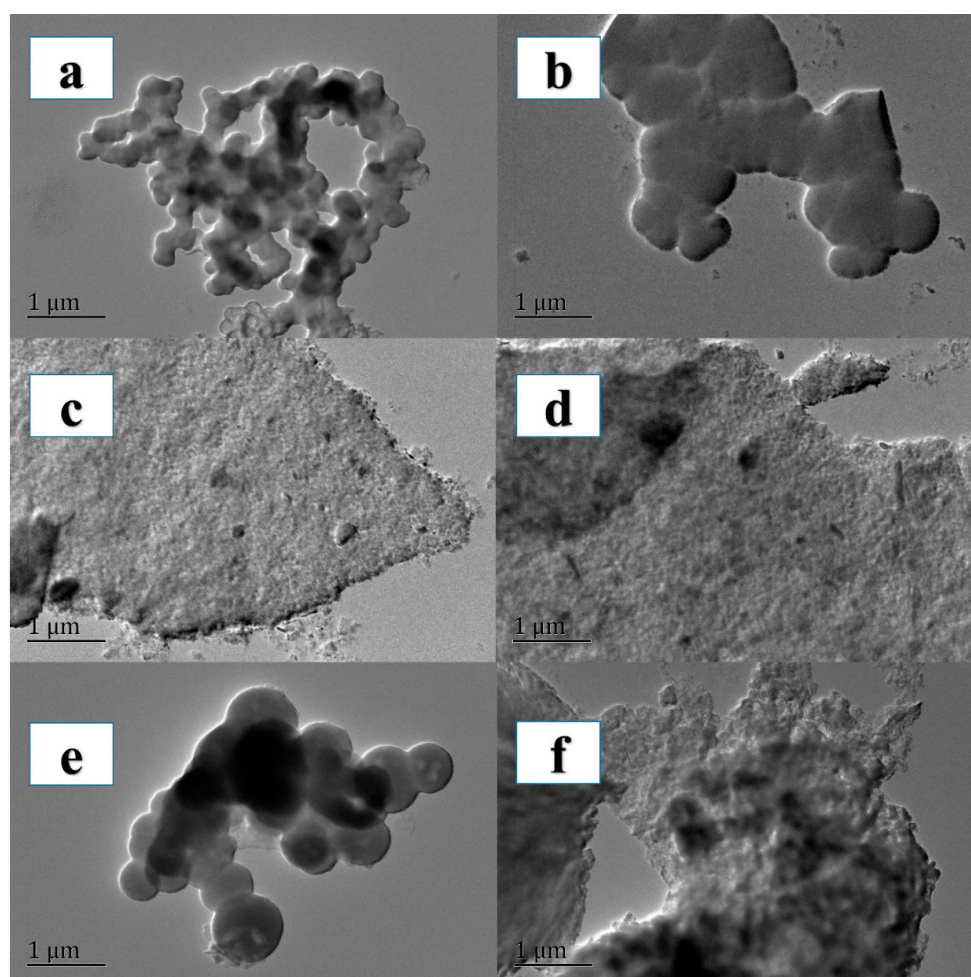


Figure 6. The figure shows transmission electron microscope (TEM) images of dissolved organic matter (DOM) being freeze-dried before and after combined with Cu^{2+} . (a). Dryland samples before being combined with Cu (b). Dryland samples after being combined with Cu, (c). forest soil samples before being combined with Cu (d). Forest soil samples after being combined with Cu (e). Vegetable field soil samples before being combined with Cu (f). Vegetable field soil samples after being combined with Cu. Cu concentration: $100 \text{ mg}\cdot\text{L}^{-1}$.

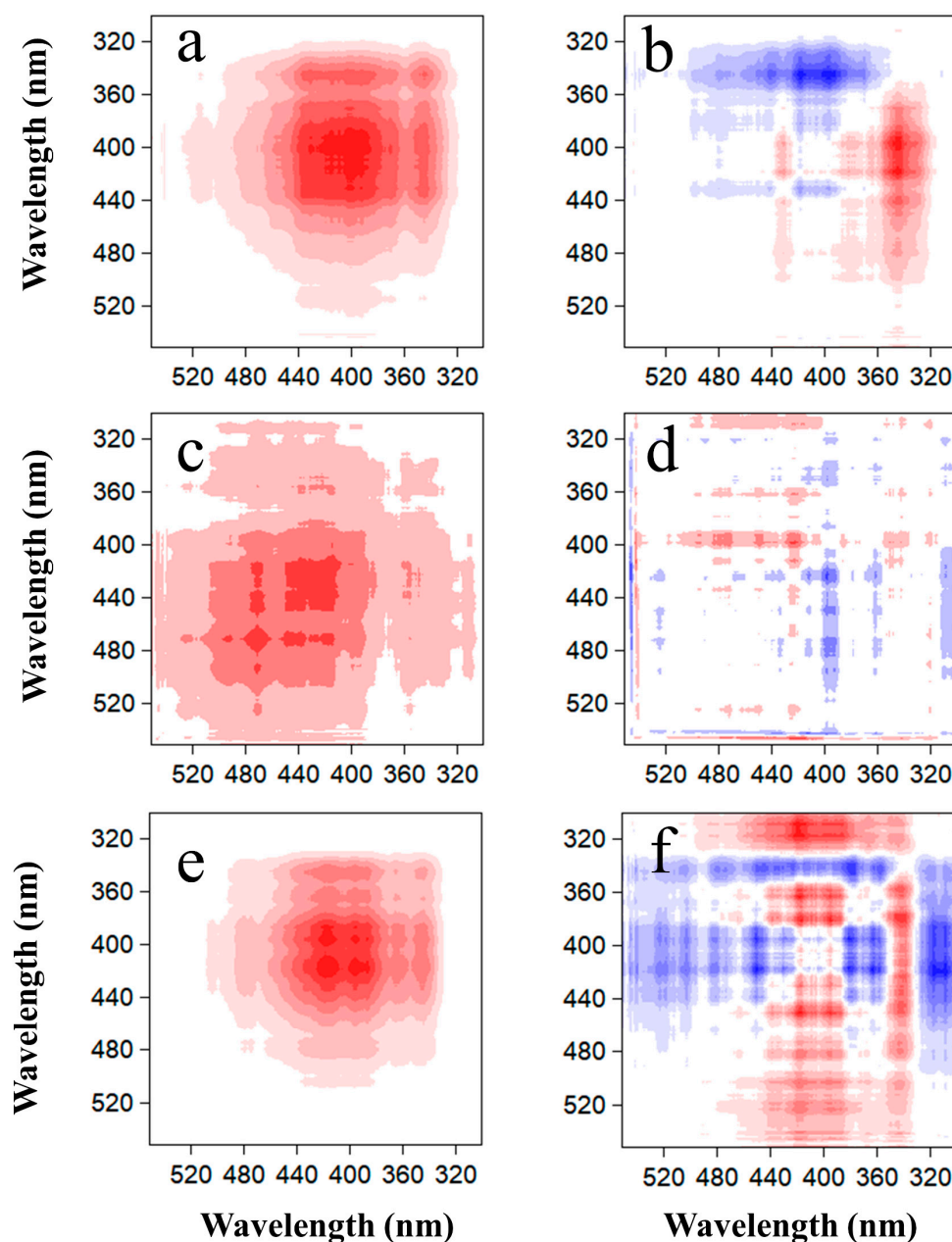


Figure 7. The figure shows synchronous and asynchronous spectra of dissolved organic matter and Cu^{2+} combinations in soils of different agricultural land types. Synchronous (a) and asynchronous (b) spectra of dry farmland, synchronous (c) and asynchronous (d) spectra of forest land, and synchronous (e) and asynchronous (f) spectra of vegetable fields.

The appearance of multiple cross-peaks in the asynchronous spectrum after the combination of forest land DOM with Cu^{2+} indicates that forest land DOM has multiple combination sites, and the combination process is complex. Additionally, the humic acid component, not identified in the three-dimensional fluorescence analysis of forest land DOM, was observed to bind with Cu^{2+} in the two-dimensional spectrum analysis, demonstrating the higher sensitivity of the two-dimensional spectrum analysis. In summary, the short-wave fulvic acid components in the DOM of three different types of agricultural soils preferentially bind with Cu^{2+} , especially with phenolic groups, hydroxyl groups, and phenolic hydroxyl groups in short-wave fulvic acid, showing higher sensitivity to Cu^{2+} [52]. This is because more hydroxyl groups, phenolic hydroxyl groups, and easily degradable components in fulvic acid can provide more combination sites for Cu^{2+} , exhibiting stronger

reactivity [53]. The different positions of the cross-peaks in the asynchronous spectra of DOM in combination with Cu^{2+} in different types of agricultural soils indicate that the combination mechanism of the same component with Cu^{2+} may vary in different types of soil DOM.

3.3.3. Variations in Elemental Species after the Combination of DOM and Cu^{2+}

Comparing the XPS spectral peaks of DOM-Cu combinations in three soil types, after the addition of Cu^{2+} , distinct Cu peaks were observed in the spectra (Figures S4a,b, S5a,b and S6a,b), indicating the adsorption of Cu onto the surface of DOM and the occurrence of a combination between DOM and Cu^{2+} . In the XPS spectra, two types of Cu were present in all three soil types, namely Cu^{2+} (934.6 and 954.6 eV) and Cu^+ (932.5 and 952.1 eV) (Figure 8). Despite Cu^{2+} being added during the experimental process, this suggests that the combination process between DOM and Cu involves not only adsorption but also a concurrent reduction process. Furthermore, in contrast to dry farmland, the spectral area of Cu^+ in forest and vegetable fields was higher than that of Cu^{2+} (forest 60.28% vs. 39.72%, vegetable field 52.39% vs. 47.61%). These results indicate a stronger reduction capability of DOM in forest and vegetable fields. To analyze the combination mechanism of DOM-Cu in three different soil types, the spectral peaks of C, O, and N were further analyzed.

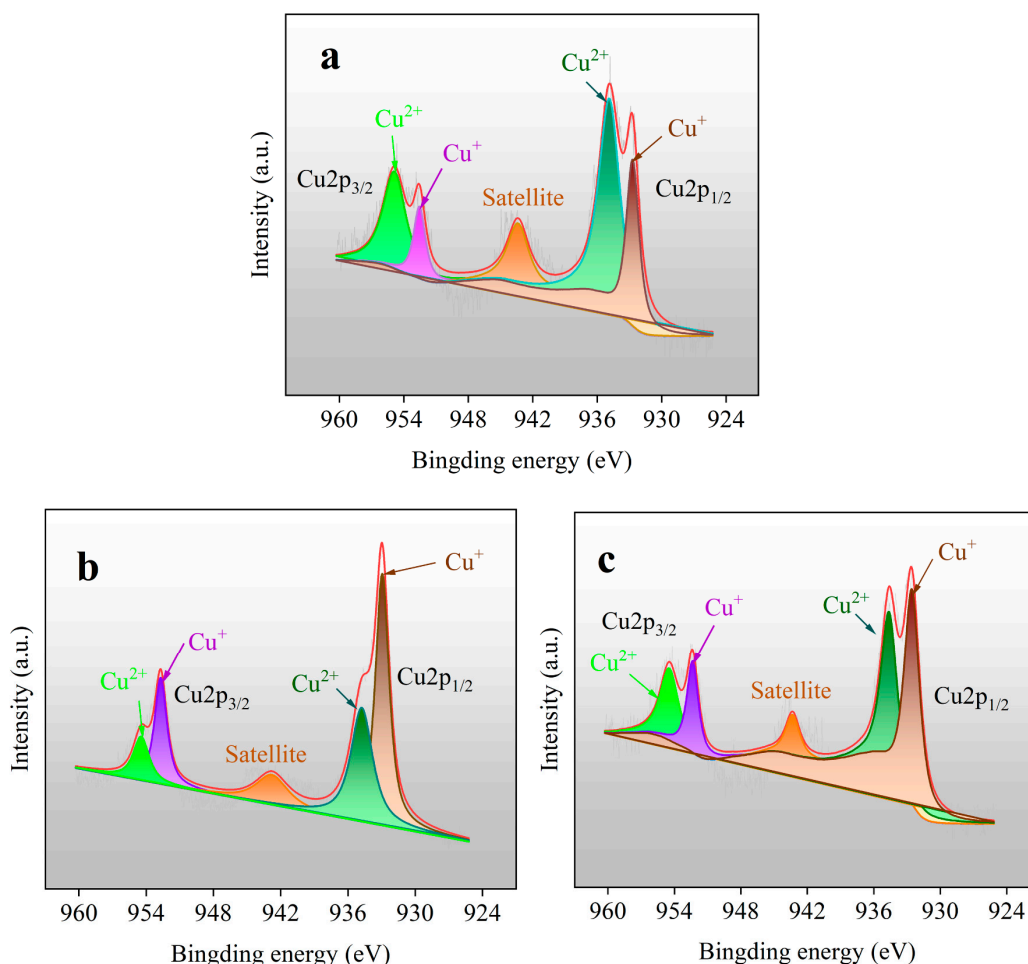


Figure 8. The figure shows the XPS spectra of Cu after the combination of dissolved organic matter with Cu^{2+} in different types of soils: (a). dry farmland, (b) forest land, and (c) vegetable fields.

In the C1s spectrum of dry farmland soil DOM, four peaks can be observed at C-O (288.7, 289.6 eV), C-H (286.4 eV), and C-C (284.8 eV), with percentages of 8.3%, 23.0%, and 69.7%, respectively (Figure S4c) [54,55]. Upon the addition of Cu^{2+} to DOM, the peak areas

of C-C and C-O decrease, while C-H increases from 23.0% to 30.0% (Figure S4d). The O1s spectrum of DOM reveals four peaks at S-O (531.9 eV), Metal-O (533.4, 532.7 eV), and H-O (531.2 eV) [56] (Figure S4e), where the peak areas of S-O and Metal-O significantly increase after the addition of Cu^{2+} (Figure S4f). The reduction in the number of N-O and C-O bonds provides conditions for the formation of Cu-O bonds. In the N1s spectrum of DOM, two peaks are observed, both corresponding to N-O (400.0, 407.4 eV) [57] (Figure S4g), with a noticeable decrease in the peak area of N-O upon the addition of Cu^{2+} (Figure S4h).

In forest soil, the C1s spectrum of DOM displays three peaks at C-O (293.2 eV) and C-H (284.5, 286.3 eV) [58] (Figure S5c), accounting for 12.0% and 88.0%, respectively. After adding Cu^{2+} to forest soil DOM, the percentage of C-H increases from 88.0% to 92.0%, while the percentage of C-O decreases from 12.0% to 8.0% (Figure S5d). Without the addition of Cu^{2+} , the O1s spectrum exhibits three peaks for S-O (530.9 eV), C-O (532.7 eV), and H-O (531.8 eV) (Figure S5e). Upon the addition of Cu^{2+} , the peak area of S-O increases, while the areas of C-O and H-O significantly decrease (Figure S5f). Without the addition of Cu^{2+} , the N1s spectrum shows only one peak at N-O (400.0 eV) (Figure S5g), but after adding Cu^{2+} , two peaks appear at N-O (400.0 eV) and $\text{N}\equiv\text{O}\equiv\text{N}$ (407.10 eV) [57] (Figure S5h). The breaking of C-O, O-H, and N-O bonds and the formation of $\text{N}\equiv\text{O}\equiv\text{N}$ contribute to the formation of Cu-O bonds.

In the C1s spectrum of vegetable field soil, three peak regions are observed. Upon the addition of Cu^{2+} to DOM, the proportions of C-C and C-O decrease, while the proportion of C-H increases (Figure S6c,d). The O1s spectrum exhibits four peaks for H-O (531.2, 531.8 eV) and C-O (533.3, 532.5 eV) [59] (Figure S6e), and after adding Cu^{2+} , the number of bonding sites for H-O and C-O decreases (Figure S6f). The breaking of H-O, C-O, and N-O bonds provides oxygen atoms for the formation of Cu-O, indicating that these Cu^{2+} primarily interact with oxygen-containing functional groups, such as hydroxyl, phenolic hydroxyl, and amino groups. Sulfur-containing functional groups in forest and vegetable field soil DOM bind to Cu^{2+} , suggesting that the reducing properties of sulfur-containing functional groups play a role in the reduction of Cu^{2+} . Additionally, after combination with Cu^{2+} , the C-H peak area in dry farmland soil increases, while in forest and vegetable field soil, it decreases. This indicates that functional groups containing C-H play a crucial role in the reduction of Cu^{2+} . For example, C-H bonds in alkenes on the DOM surface are prone to hydrogenation reactions and participate in reduction reactions. C-H bonds around carbonyl and hydroxyl groups in carboxylic acids can also participate in reduction reactions. In forest and vegetable fields, long-term redox alternations result in the presence of reductive properties in the humic acids contained in DOM. Humic acids contain quinone, phenol, and other redox functional groups, which under realistic environmental conditions, exhibit some reducing abilities toward variable-valence metals. Simultaneously, humic acids can tightly bind to the redox pair of Cu^{2+} , indirectly reducing Cu^{2+} [60,61].

4. Conclusions

In conclusion, the aromaticity and hydrophobicity of DOM differed significantly between soil types. Forest soils showed higher SUVA_{254} (9.12 ± 0.03) and SUVA_{260} (8.75 ± 0.03) values compared to dryland and vegetable soils, suggesting a higher content of aromatic compounds and hydrophobic components in forest soils. While the fluorescence peaks were similar for dryland and vegetable soils, forest soils showed different fluorescence patterns, suggesting differences in the source and composition of DOM and showing a higher degree of organic matter decomposition and aromaticity compared to other soil types. Humic-like acids preferentially combined with Cu^{2+} in dry farmland and vegetable field soils, and the humic-like fraction had a stronger combination affinity for Cu^{2+} than the fulvic-like fraction ($\lg K_M$ 4.88 vs. 4.51; $\lg K_M$ 5.21 vs. 4.90). Short-wave humic acid components in soil DOM bind preferentially to Cu^{2+} , and forest DOM has more combination sites with Cu^{2+} . In addition, Cu^{2+} species complex with oxygen-containing functional groups such as hydroxyl, phenolic hydroxyl, and amino groups in agricultural soil DOM. Furthermore, DOM from agricultural, forest and vegetable field soils contains

sulphur-containing functional groups and C-H functional groups, which contribute to stronger reducing capacities. According to this study, the combination of DOM to Cu^{2+} can be enhanced by increasing the humic acid content of the soil by adding humus or by increasing the level of decomposition of organic matter during agricultural production activities. Furthermore, it is important to pay attention to the effects of Cu^{2+} valence transition on crops during soil tillage and fertilisation processes. This comprehensive analysis provides valuable insights into the composition, structure, and interaction of DOM with Cu in different agricultural soils, helping us to understand the dynamics of soil organic matter and its impact on environmental processes and the fate of contaminants.

Supplementary Materials: The following are available online at <https://www.mdpi.com/article/10.3390/agriculture14050684/s1>, Figure S1: Fluorescence quenching process of dissolved organic matter (DOM) in dryland soil under different Cu^{2+} concentrations. Cu^{2+} concentration (a). 0, (b). 5, (c). 10, (d). 20, (e). 30, (f). 50, (g). 75, and (h). $100 \mu\text{mol}\cdot\text{L}^{-1}$. Figure S2: Fluorescence quenching process of dissolved organic matter (DOM) in forest soil under different Cu^{2+} concentrations. Cu^{2+} concentration (a). 0, (b). 5, (c). 10, (d). 20, (e). 30, (f). 50, (g). 75, and (h). $100 \mu\text{mol}\cdot\text{L}^{-1}$. Figure S3: Fluorescence quenching process of soil dissolved organic matter (DOM) in vegetable fields under different Cu^{2+} concentrations. Cu^{2+} concentration (a). 0, (b). 5, (c). 10, (d). 20, (e). 30, (f). 50, (g). 75, and (h). $100 \mu\text{mol}\cdot\text{L}^{-1}$. Figure S4: XPS spectra of dissolved organic matter (DOM) of dry farmland soil before and after combination with Cu^{2+} . (a,b). Full XPS spectra of without and with DOM combination with Cu^{2+} ; (c–h) were C, O, and N spectra of DOM without and with DOM combination with Cu^{2+} , respectively. Figure S5: XPS spectra of dissolved organic matter (DOM) of forest land soil before and after combination with Cu^{2+} . (a,b). Full XPS spectra of without and with DOM combination with Cu^{2+} ; (c–h) were C, O, and N spectra of DOM without and with DOM combination with Cu^{2+} , respectively. Figure S6: XPS spectra of dissolved organic matter (DOM) of vegetable fields soil before and after combination with Cu^{2+} . (a,b). Full XPS spectra of without and with DOM combination with Cu^{2+} ; (c–h) were C, O, and N spectra of DOM without and with DOM combination with Cu^{2+} , respectively. Table S1: Characterisation of dissolved organic matter using spectral analysis; Table S2: Fluorescence spectral parameters of dissolved organic matter in soil of different agricultural land types.

Author Contributions: Conceptualisation, Y.Y., J.L. and S.L.; methodology, Y.Y., J.Z. and X.H.; software, K.M.; validation, Y.L. and F.F.; formal analysis, Y.Y.; investigation, X.H.; resources, S.L.; data curation, Y.W.; writing—original draft preparation, Y.Y.; writing—review and editing, J.L. and S.L.; visualisation, K.M.; supervision, Y.Y.; project administration, F.F.; funding acquisition, Y.Y. and S.L. All authors have read and agreed to the published version of the manuscript.

Funding: This research was funded by the National Natural Science Foundation of China (Grant Nos. 42207454, 51979137, 41977402), Natural Science Research Project of Anhui Educational Committee (KJ2021A0121), Applied Basic Research Project of Wuhu (2022jc09), and Ph.D research start-up fund (762140) and talent cultivation project (2021xjxm032) of Anhui Normal University, China National University Student Innovation & Entrepreneurship Development Program (202310370054).” and The APC was funded by the National Natural Science Foundation of China (Grant No. 42207454).

Institutional Review Board Statement: Not applicable.

Data Availability Statement: Data will be made available on request.

Conflicts of Interest: The authors declare no conflicts of interest.

References

1. Kríbek, B.; Sípková, A.; Ettler, V.; Mihaljevic, M.; Majer, V.; Knésl, I.; Mapani, B.; Penížek, V.; Vanek, A.; Sracek, O. Variability of the copper isotopic composition in soil and grass affected by mining and smelting in Tsumeb, Namibia. *Chem. Geol.* **2018**, *493*, 121–135. [[CrossRef](#)]
2. Chen, L.; Zhou, M.X.; Wang, J.Z.; Zhang, Z.Q.; Duan, C.J.; Wang, X.X.; Zhao, S.L.; Bai, X.H.; Li, Z.J.; Li, Z.M.; et al. A global meta-analysis of heavy metal(loid)s pollution in soils near copper mines: Evaluation of pollution level and probabilistic health risks. *Sci. Total Environ.* **2022**, *835*, 155441. [[CrossRef](#)] [[PubMed](#)]
3. Rizvi, A.; Khan, M.S. Heavy metal induced oxidative damage and root morphology alterations of maize (*Zea mays* L.) plants and stress mitigation by metal tolerant nitrogen fixing *Azotobacter chroococcum*. *Ecotox. Environ. Safe.* **2018**, *157*, 9–20. [[CrossRef](#)] [[PubMed](#)]

4. Napolitano, P.; Guezgouz, N.; Benradia, I.; Benredjem, S.; Parisi, C.; Guerriero, G.; De Marco, A. Non-Lethal Assessment of Land Use Change Effects in Water and Soil of Algerian Riparian Areas along the Medjerda River through the Biosentinel *Bufo spinosus* Daudin. *Water* **2024**, *16*, 538. [[CrossRef](#)]
5. Mitra, G.; Mukhopadhyay, P.K.; Ayyappan, S. Biochemical composition of zooplankton community grown in freshwater earthen ponds: Nutritional implication in nursery rearing of fish larvae and early juveniles. *Aquaculture* **2007**, *272*, 346–360. [[CrossRef](#)]
6. Chiang, C.T.; Lian, I.B.; Su, C.C.; Tsai, K.Y.; Lin, Y.P.; Chang, T.K. Spatiotemporal Trends in Oral Cancer Mortality and Potential Risks Associated with Heavy Metal Content in Taiwan Soil. *Int. J. Environ. Res. Public Health* **2010**, *7*, 3916–3928. [[CrossRef](#)] [[PubMed](#)]
7. Coelho, C.; Foret, C.; Bazin, C.; Leduc, L.; Hammada, M.; Inácio, M.; Bedell, J.P. Bioavailability and bioaccumulation of heavy metals of several soils and sediments (from industrialized urban areas) for *Eisenia fetida*. *Sci. Total Environ.* **2018**, *635*, 1317–1330. [[CrossRef](#)] [[PubMed](#)]
8. Yao, Y.R.; Ma, K.; Li, S.Y.; Zhang, Y.; Zhang, Z.M.; Fang, F.M.; Lin, Y.S.; Yin, L.; Sun, L.; Zhang, C.H. Dissolved organic matter and Fe/Mn enhance the combination and transformation of As in Lake Chaohu Basin. *J. Environ. Manag.* **2024**, *349*, 119425. [[CrossRef](#)]
9. Ge, B.M.; Zhou, J.; Yang, R.P.; Jiang, S.H.; Yang, L.; Tang, B.P. Lower land use intensity promoted soil macrofaunal biodiversity on a reclaimed coast after land use conversion. *Agric. Ecosyst. Environ.* **2021**, *306*, 107208. [[CrossRef](#)]
10. Sharifi, A.; Shirani, H.; Besalatpour, A.A.; Esfandiarpour-Boroujeni, I.; Hajabbasi, M.A. High-energy moisture characteristics of various low organic matter sandy soils in different land uses. *Geoderma* **2021**, *398*, 115104. [[CrossRef](#)]
11. Chen, H.; Kong, W.D.; Shi, Q.; Wang, F.; He, C.; Wu, J.S.; Lin, Q.M.; Zhang, X.Z.; Zhu, Y.G.; Liang, C.; et al. Patterns and drivers of the degradability of dissolved organic matter in dryland soils on the Tibetan Plateau. *J. Appl. Ecol.* **2022**, *59*, 884–894. [[CrossRef](#)]
12. Zhang, Q.; Wang, Y.H.; Guan, P.; Zhang, P.; Mo, X.H.; Yin, G.G.; Qu, B.; Xu, S.J.; He, C.; Shi, Q.; et al. Temperature Thresholds of Pyrogenic Dissolved Organic Matter in Heating Experiments Simulating Forest Fires. *Environ. Sci. Technol.* **2023**, *57*, 17291–17301. [[CrossRef](#)]
13. Yuan, X.C.; Cui, J.Y.; Wu, L.Z.; Liu, C.C.; Zhang, Q.F.; Zeng, Q.X.; Zhou, J.C.; Lin, K.M.; Wu, Y.; Lin, H.Y.; et al. Relationship between soil bacterial communities and dissolved organic matter in a subtropical *Pinus taiwanensis* forest after short-term nitrogen addition. *Forest. Ecol. Manag.* **2022**, *512*, 120165. [[CrossRef](#)]
14. Yang, Y.; Geng, J.; Cheng, S.L.; Fang, H.J.; Guo, Y.F.; Li, Y.A.; Zhou, Y.; Shi, F.Y.; Vancampenhout, K. Linking soil microbial community to the chemical composition of dissolved organic matter in a boreal forest during freeze-thaw cycles. *Geoderma* **2023**, *431*, 116359. [[CrossRef](#)]
15. Yuan, X.C.; Cui, J.Y.; Lin, K.M.; Liu, C.C.; Zhou, J.C.; Zhang, Q.F.; Zeng, Q.X.; Wu, L.Z.A.; Wu, Y.; Mei, K.C.; et al. Effects of nitrogen addition on the concentration and composition of soil-based dissolved organic matter in subtropical *Pinus taiwanensis* forests. *J. Soils Sediments* **2022**, *22*, 1924–1937. [[CrossRef](#)]
16. Pan, H.W.; Shi, L.L.; Liu, X.; Lei, H.J.; Yang, G.; Chen, H.R. Interactions Between Humic Acid and the Forms and Bioavailability of Copper in Water. *Water Air Soil Poll.* **2023**, *234*, 312. [[CrossRef](#)]
17. Jiang, S.J.; Dai, G.L.; Liu, Z.Y.; He, T.; Zhong, J.; Ma, Y.C.; Shu, Y.H. Field-scale fluorescence fingerprints of biochar-derived dissolved organic matter (DOM) provide an effective way to trace biochar migration and the downward co-migration of Pb, Cu and As in soil. *Chemosphere* **2022**, *301*, 134738. [[CrossRef](#)]
18. Guo, X.J.; Peng, Y.Y.; Li, N.X.; Tian, Y.Y.; Dai, L.C.; Wu, Y.; Huang, Y. Effect of biochar-derived DOM on the interaction between Cu(II) and biochar prepared at different pyrolysis temperatures. *J. Hazard. Mater.* **2022**, *421*, 126739. [[CrossRef](#)]
19. da Silva, L.S.; Constantino, I.C.; Bento, L.R.; Tadini, A.M.; Bisinoti, M.C.; Boscolo, M.; Ferreira, O.P.; Mounier, S.; Piccolo, A.; Spaccini, R.; et al. Humic extracts from hydrochar and Amazonian Anthrosol: Molecular features and metal binding properties using EEM-PARAFAC and 2D FTIR correlation analyses. *Chemosphere* **2020**, *256*, 127110. [[CrossRef](#)]
20. Hu, S.H.; Lu, C.; Zhang, C.J.; Zhang, Y.J.; Yao, H.R.; Wu, Y.G. Effects of fresh and degraded dissolved organic matter derived from maize straw on copper sorption onto farmland loess. *J. Soils Sediments* **2016**, *16*, 327–338. [[CrossRef](#)]
21. Araújo, E.; Strawn, D.G.; Morra, M.; Moore, A.; Alleoni, L.R.F. Association between extracted copper and dissolved organic matter in dairy-manure amended soils. *Environ. Pollut.* **2019**, *246*, 1020–1026. [[CrossRef](#)] [[PubMed](#)]
22. Guo, X.J.; He, X.S.; Li, C.W.; Li, N.X. The binding properties of copper and lead onto compost-derived DOM using Fourier-transform infrared, UV-vis and fluorescence spectra combined with two-dimensional correlation analysis. *J. Hazard. Mater.* **2019**, *365*, 457–466. [[CrossRef](#)] [[PubMed](#)]
23. Andersson, E.; Meklesh, V.; Gentile, L.; Bhattacharya, A.; Stålblbrand, H.; Tunlid, A.; Persson, P.; Olsson, U. Generation and properties of organic colloids extracted by water from the organic horizon of a boreal forest soil. *Geoderma* **2023**, *432*, 116386. [[CrossRef](#)]
24. Ohno, T.; Fernandez, I.J.; Hiradate, S.; Sherman, J.F. Effects of soil acidification and forest type on water soluble soil organic matter properties. *Geoderma* **2007**, *140*, 176–187. [[CrossRef](#)]
25. Ren, H.Y.; Ma, F.Y.; Yao, X.; Shao, K.Q.; Yang, L.W. Multi-spectroscopic investigation on the spatial distribution and copper binding ability of sediment dissolved organic matter in Nansi Lake, China. *J. Hydrol.* **2020**, *591*, 125289. [[CrossRef](#)]
26. Wu, J.; Zhang, H.; He, P.J.; Shao, L.M. Insight into the heavy metal binding potential of dissolved organic matter in MSW leachate using EEM quenching combined with PARAFAC analysis. *Water Res.* **2011**, *45*, 1711–1719. [[CrossRef](#)] [[PubMed](#)]

27. Liu, D.P.; Gao, H.J.; Yu, H.B.; Song, Y.H. Applying EEM-PARAFAC combined with moving-window 2DCOS and structural equation modeling to characterize binding properties of Cu (II) with DOM from different sources in an urbanized river. *Water Res.* **2022**, *227*, 119317. [[CrossRef](#)] [[PubMed](#)]
28. Wang, K.F.; Zhao, Y.F.; Yang, Z.W.; Lin, Z.M.; Tan, Z.Y.; Du, L.; Liu, C.L. Concentration and characterization of groundwater colloids from the northwest edge of Sichuan basin, China. *Colloid. Surf. A* **2018**, *537*, 85–91. [[CrossRef](#)]
29. Noda, I.; Dowrey, A.E.; Marcott, C.; Story, G.M.; Ozaki, Y. Generalized two-dimensional correlation spectroscopy. *Appl. Spectrosc.* **2000**, *54*, 236A–248A. [[CrossRef](#)]
30. Berry, R.J.; Ozaki, Y. Comparison of wavelets and smoothing for denoising spectra for two-dimensional correlation spectroscopy. *Appl. Spectrosc.* **2002**, *56*, 1462–1469. [[CrossRef](#)]
31. Lu, X.Q.; Jaffe, R. Interaction between Hg(II) and natural dissolved organic matter: A fluorescence spectroscopy based study. *Water Res.* **2001**, *35*, 1793–1803. [[CrossRef](#)] [[PubMed](#)]
32. Yeh, Y.L.; Yeh, K.J.; Hsu, L.F.; Yu, W.C.; Lee, M.H.; Chen, T.C. Use of fluorescence quenching method to measure sorption constants of phenolic xenoestrogens onto humic fractions from sediment. *J. Hazard. Mater.* **2014**, *277*, 27–33. [[CrossRef](#)] [[PubMed](#)]
33. Miersch, T.; Czech, H.; Hartikainen, A.; Ihalainen, M.; Orasche, J.; Abbaszade, G.; Tissari, J.; Streibel, T.; Jokiniemi, J.; Sippula, O.; et al. Impact of photochemical ageing on Polycyclic Aromatic Hydrocarbons (PAH) and oxygenated PAH (Oxy-PAH/OH-PAH) in logwood stove emissions. *Sci. Total Environ.* **2019**, *686*, 382–392. [[CrossRef](#)] [[PubMed](#)]
34. Selberg, A.; Viik, M.; Ehapalu, K.; Tenno, T. Content and composition of natural organic matter in water of Lake Pitkjarv and mire feeding Kuke River (Estonia). *J. Hydrol.* **2011**, *400*, 274–280. [[CrossRef](#)]
35. Martin, D.; Srivastava, P.C.; Ghosh, D.; Zech, W. Characteristics of humic substances in cultivated and natural forest soils of Sikkim. *Geoderma* **1998**, *84*, 345–362. [[CrossRef](#)]
36. Fialho, L.L.; da Silva, W.T.L.; Milori, D.; Simoes, M.L.; Martin-Neto, L. Characterization of organic matter from composting of different residues by physicochemical and spectroscopic methods. *Bioresour. Technol.* **2010**, *101*, 1927–1934. [[CrossRef](#)] [[PubMed](#)]
37. Bai, Y.C.; Wu, F.C.; Xing, B.S.; Meng, W.; Shi, G.L.; Ma, Y.; Giesy, J.P. Isolation and Characterization of Chinese Standard Fulvic Acid Sub-fractions Separated from Forest Soil by Stepwise Elution with Pyrophosphate Buffer. *Sci. Rep.-UK* **2015**, *5*, 8723. [[CrossRef](#)] [[PubMed](#)]
38. Artinger, R.; Buckau, G.; Geyer, S.; Fritz, P.; Wolf, M.; Kim, J.I. Characterization of groundwater humic substances: Influence of sedimentary organic carbon. *Appl. Geochem.* **2000**, *15*, 97–116. [[CrossRef](#)]
39. Nguyen, H.V.M.; Hur, J. Tracing the sources of refractory dissolved organic matter in a large artificial lake using multiple analytical tools. *Chemosphere* **2011**, *85*, 782–789. [[CrossRef](#)]
40. Zhao, C.; Wang, C.C.; Li, J.Q.; Wang, P.; Ou, J.Q.; Cui, J.R. Interactions between copper(II) and DOM in the urban stormwater runoff: Modeling and characterizations. *Environ. Technol.* **2018**, *39*, 120–129. [[CrossRef](#)]
41. Kiikkilä, O.; Smolander, A.; Kitunen, V. Degradability, molecular weight and adsorption properties of dissolved organic carbon and nitrogen leached from different types of decomposing litter. *Plant Soil* **2013**, *373*, 787–798. [[CrossRef](#)]
42. Zhang, X.Q.; Li, Y.; Li, Y.; Ye, J.; Chen, Z.H.; Ren, D.J.; Zhang, S.Q. The spectral characteristics and cadmium complexation of soil dissolved organic matter in a wide range of forest lands. *Environ. Pollut.* **2022**, *299*, 118834. [[CrossRef](#)] [[PubMed](#)]
43. Li, M.; Drosos, M.; Hu, H.L.; He, X.S.; Wang, G.X.; Zhang, H.; Hu, Z.Y.; Xi, B.D. Organic amendments affect dissolved organic matter composition and mercury dissolution in pore waters of mercury-polluted paddy soil. *Chemosphere* **2019**, *232*, 356–365. [[CrossRef](#)] [[PubMed](#)]
44. Korak, J.A.; Wert, E.C.; Rosario-Ortiz, F.L. Evaluating fluorescence spectroscopy as a tool to characterize cyanobacteria intracellular organic matter upon simulated release and oxidation in natural water. *Water Res.* **2015**, *68*, 432–443. [[CrossRef](#)] [[PubMed](#)]
45. Yao, Y.L.; Zhao, W.H.; Miao, H. Studied on Colored Dissolved Organic Matter of Spring in North Yellow Sea with Three-Dimensional Fluorescence Spectroscopy Combined with Parallel Factor Analysis. *Spectrosc. Spect. Anal.* **2016**, *36*, 2532–2537.
46. De Mastro, F.; Cocozza, C.; Traversa, A.; Savy, D.; Abdelrahman, H.M.; Brunetti, G. Influence of crop rotation, tillage and fertilization on chemical and spectroscopic characteristics of humic acids. *PLoS ONE* **2019**, *14*, e0219099. [[CrossRef](#)] [[PubMed](#)]
47. Ohno, T.; Hess, N.J.; Qafoku, N.P. Current Understanding of the Use of Alkaline Extractions of Soils to Investigate Soil Organic Matter and Environmental Processes. *J. Environ. Qual.* **2019**, *48*, 1561–1564. [[CrossRef](#)]
48. Phungsai, P.; Kurisu, F.; Kasuga, I.; Furumai, H. Changes in dissolved organic matter during water treatment by sequential solid-phase extraction and unknown screening analysis. *Chemosphere* **2021**, *263*, 128278. [[CrossRef](#)]
49. Wu, J.; Zhang, H.; Yao, Q.S.; Shao, L.M.; He, P.J. Toward understanding the role of individual fluorescent components in DOM-metal binding. *J. Hazard. Mater.* **2012**, *215*, 294–301. [[CrossRef](#)]
50. Plaza, C.; Brunetti, G.; Senesi, N.; Polo, A. Molecular and quantitative analysis of metal ion binding to humic acids from sewage sludge and sludge-amended soils by fluorescence spectroscopy. *Environ. Sci. Technol.* **2006**, *40*, 917–923. [[CrossRef](#)]
51. Wei, J.; Tu, C.; Yuan, G.D.; Liu, Y.; Bi, D.X.; Xiao, L.; Lu, J.; Theng, B.K.G.; Wang, H.L.; Zhang, L.J.; et al. Assessing the effect of pyrolysis temperature on the molecular properties and copper sorption capacity of a halophyte biochar. *Environ. Pollut.* **2019**, *251*, 56–65. [[CrossRef](#)] [[PubMed](#)]
52. Chen, W.; Habibul, N.; Liu, X.Y.; Sheng, G.P.; Yu, H.Q. FTIR and Synchronous Fluorescence Heterospectral Two-Dimensional Correlation Analyses on the Binding Characteristics of Copper onto Dissolved Organic Matter. *Environ. Sci. Technol.* **2015**, *49*, 2052–2058. [[CrossRef](#)] [[PubMed](#)]

53. Baken, S.; Degryse, F.; Verheyen, L.; Merckx, R.; Smolders, E. Metal Complexation Properties of Freshwater Dissolved Organic Matter Are Explained by Its Aromaticity and by Anthropogenic Ligands. *Environ. Sci. Technol.* **2011**, *45*, 2584–2590. [[CrossRef](#)] [[PubMed](#)]
54. Lan, N.; Yang, W.; Gao, W.; Guo, P.; Zhao, C.; Chen, J. Characterization of ta-C film on micro arc oxidation coated titanium alloy in simulated seawater. *Diam. Relat. Mater.* **2021**, *117*, 108483. [[CrossRef](#)]
55. Biesinger, M.C.; Lau, L.W.M.; Gerson, A.R.; Smart, R.S.C. Resolving surface chemical states in XPS analysis of first row transition metals, oxides and hydroxides: Sc, Ti, V, Cu and Zn. *Appl. Surf. Sci.* **2010**, *257*, 887–898. [[CrossRef](#)]
56. Fetisov, A.V.; Kozhina, G.A.; Estemirova, S.K.; Fetisov, V.B.; Mitrofanov, V.Y.; Uporov, S.A.; Vedmid, L.B. XPS Study of Mechanically Activated $\text{YBa}_2\text{Cu}_3\text{O}_{6+\delta}$ and $\text{NdBa}_2\text{Cu}_3\text{O}_{6+\delta}$. *J. Spectrosc.* **2013**, *2013*, 217268. [[CrossRef](#)]
57. Zhang, J.R.; Ma, Y.; Wang, S.Y.; Ding, J.F.; Gao, B.; Kan, E.; Hua, W.J. Accurate K-edge X-ray photoelectron and absorption spectra of g- C_3N_4 nanosheets by first-principles simulations and reinterpretations. *Phys. Chem. Phys.* **2019**, *21*, 22819–22830. [[CrossRef](#)]
58. Biesinger, M.C.; Payne, B.P.; Grosvenor, A.P.; Lau, L.W.M.; Gerson, A.R.; Smart, R.S. Resolving surface chemical states in XPS analysis of first row transition metals, oxides and hydroxides: Cr, Mn, Fe, Co and Ni. *Appl. Surf. Sci.* **2011**, *257*, 2717–2730. [[CrossRef](#)]
59. Yu, G.H.; Wu, M.J.; Wei, G.R.; Luo, Y.H.; Ran, W.; Wang, B.R.; Zhang, J.C.; Shen, Q.R. Binding of Organic Ligands with Al(III) in Dissolved Organic Matter from Soil: Implications for Soil Organic Carbon Storage. *Environ. Sci. Technol.* **2012**, *46*, 6102–6109. [[CrossRef](#)]
60. Huang, Y.N.; Qian, T.T.; Dang, F.; Yin, Y.G.; Li, M.; Zhou, D.M. Significant contribution of metastable particulate organic matter to natural formation of silver nanoparticles in soils. *Nat. Commun.* **2019**, *10*, 3775. [[CrossRef](#)]
61. Voelker, B.M.; Morel, F.M.M.; Sulzberger, B. Iron redox cycling in surface waters: Effects of humic substances and light. *Environ. Sci. Technol.* **1997**, *31*, 1004–1011. [[CrossRef](#)]

Disclaimer/Publisher’s Note: The statements, opinions and data contained in all publications are solely those of the individual author(s) and contributor(s) and not of MDPI and/or the editor(s). MDPI and/or the editor(s) disclaim responsibility for any injury to people or property resulting from any ideas, methods, instructions or products referred to in the content.